FERMILAB-FN-0795-E

Search for Single Top Quark Production at DØ in Run II

Reinhard Schwienhorst*
Department of Physics & Astronomy, Michigan State University, East Lansing, MI 48824, USA
(Dated: April 29, 2005)

I present a comprehensive search for electroweak production of single top quarks in Run II at the Fermilab Tevatron at $\sqrt{s}$ =1.96TeV. Using 230 pb^{-1} of data collected with the DØ experiment, searches for s-channel and t-channel single top quark production have been carried out in the electron+jets and muon+jets decay channels using secondary-vertex b-quark tagging to select signal-like events. A binned likelihood has been constructed from the outputs of neural networks in order to maximize the sensitivity to single top quark production. No evidence for a single top quark signal is found. However, the 95% confidence level upper limits on the production cross section of 6.4 pb in the s-channel and 5.0 pb in the t-channel are improvements over previous limits by a factor of two and are approaching the cross section region predicted by the standard model.

INTRODUCTION

The top quark is by far the heaviest and most elusive fermion in the standard model (SM). Its large mass, and coupling strength to the Higgs boson of order unity, suggests a connection between the top quark and the physics of electroweak symmetry breaking (the origin of mass). In particular, the electroweak interaction of the top quark with the W boson is the key to predicting the Higgs boson mass within the SM. However, very little is currently known experimentally about the electroweak interaction of the top quark or the Wtb vertex. Significant advances in our understanding of the Wtb vertex can be made in the near future by studying the electroweak production of single top quarks at the Tevatron. In fact, observing and studying this interaction is one of the most important subjects for the Fermilab Tevatron proton-antiproton collider in Run II. Moreover, even before the observation of electroweak single top quark production, setting sufficiently tight limits on the production cross section will serve to constrain several extensions to the SM that would enhance the single top quark production cross section. The analysis described here is the first to be able to do this in a meaningful way. The advanced analysis methods employed here also set the stage for future searches on larger datasets.

The top quark was discovered by the CDF and DØ collaborations [1, 2] in 1995 at the Fermilab Tevatron proton-antiproton colliders as top-antitop pairs. The SM predicts that the top quark is also produced singly at hadron colliders through the electroweak charged current interaction, but this production process has not yet been observed. A measurement of the single top quark production cross section will provide the first direct measurement of the CKM matrix element V_{tb} because the production cross section is proportional to $|V_{tb}|^2$. By contrast, all of the existing constraints on V_{tb} have been derived indirectly, assuming three quark generations and unitarity of the CKM matrix. Once single top quark production has been observed, a study of spin correlations in single top quark production can be used to test the $V-A$ structure of the top quark charged-current weak interaction. The single top quark final state is also predicted by several different models of new physics, and studying single top quark production is a sensitive probe to new physics [3], making it possible to rule out many models of new physics even before reaching sensitivity to the standard model cross section. It is also a significant background to SM Higgs searches at the Tevatron in the associated production process $q\bar{q}' \to WH$ with decay $H \to b\bar{b}$ [4–6] and other new physics searches [7].

Shown in Fig. 1 are the s-channel decay of a virtual W boson, leading to the final state of a top quark and a bottom quark ($t\bar{b}$), and the t-channel exchange of a virtual W between a light quark and a bottom quark, leading to a final state of a top quark and a light quark (tq). Single top quarks are also produced in association with a W boson (tW^-), but with a cross section too small to be observed at the Tevatron.

Of the single top quark production processes, the one with the largest production cross section at the Tevatron at $\sqrt{s} = 1.96$ TeV is due to the t-channel exchange, for which calculations at next-to-leading order (NLO) in the strong coupling constant (α_s) yield a production cross section of 1.98 pb [8, 9]. The next largest cross section is from the s-channel, for which NLO calculations predict a cross section of 0.88 pb [8, 9].

In Run I at the Tevatron, searches for single top quark production were performed by both CDF [10] and DØ [11]. At the 95% confidence level, the CDF limit on the s-channel production cross section is 18 pb and that of DØ is 17 pb. At the same confidence level, the CDF limit on the t-channel production cross section is 13 pb and that of DØ is 22 pb. Recent searches for single top quark production in Run II at the Tevatron have yielded limits from CDF of 13.6 pb in the s-channel and 10.1 pb in the t-channel [12].

This paper presents a first comprehensive search for single top quark production at DØ, optimized separately for the s-channel and the t-channel. It is organized as follows: First, an analysis of the s-channel and t-channel single top quark processes at the parton level at NLO

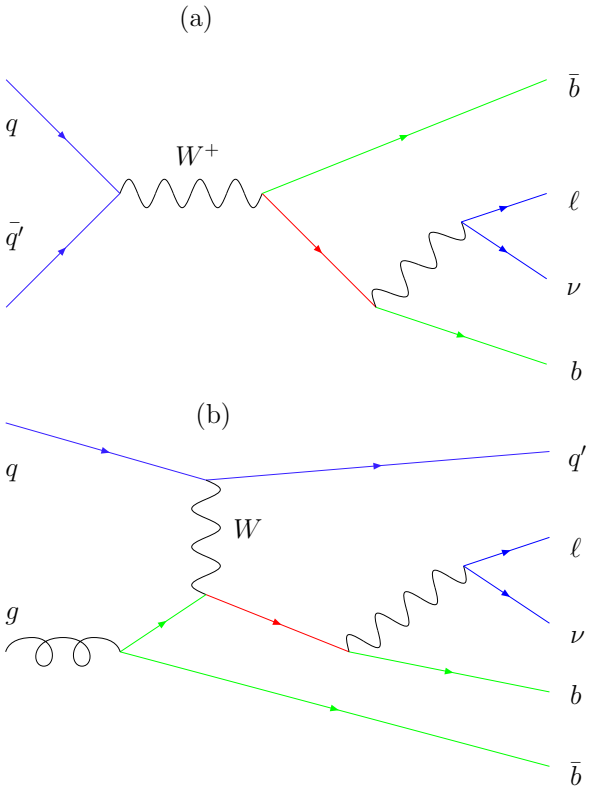

Figure 1: Feynman diagrams for single top quark production and decay for the s-channel (a) and the t-channel (b). The $\bar{b}$ quark from initial state radiation in the t-channel is included in the diagram (b).

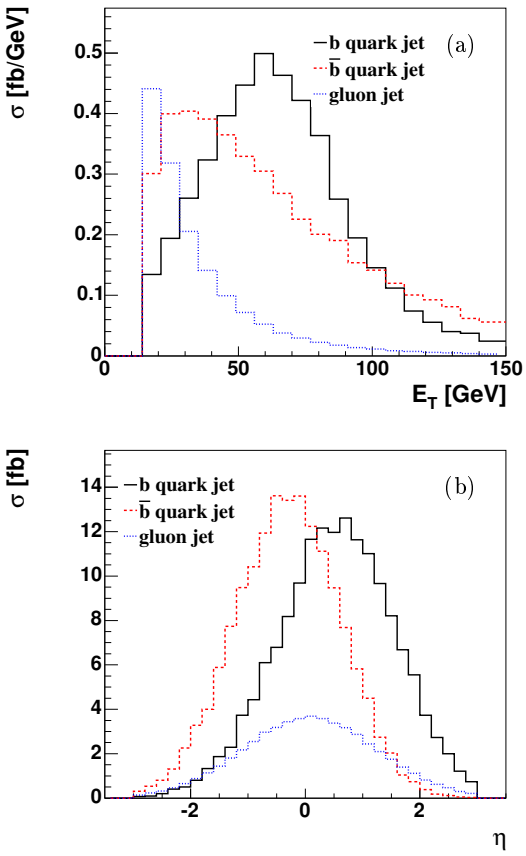

Figure 2: Transverse energy (a) and pseudo-rapidity (b) distribution of final state jets at NLO for the s-channel, after selection cuts.

is presented. Second, the DØ detector and the single top quark event selection are described. That is followed by an overview of the variables discriminating signal and background and their combination in neural networks. A description of the statistical analysis of the neural network outputs is then followed by a summary of the result.

PARTON LEVEL STUDY

This section discusses the final state signature of single top quark interactions at the parton level. The s-channel final state (Fig. 1 (a)) consists of the lepton and neutrino from the W boson arising from the top quark decay, the b quark from the top quark decay, and the $\bar{b}$ quark produced together with the top quark. The t-channel final state (Fig. 1 (b)) consists of the same top quark decay products (lepton, neutrino, b quark) and a light quark produced with the top quark. Furthermore, since the t-channel has an initial state b quark, there is also a $\bar{b}$ quark produced from initial state radiation, although this quark typically appears at low transverse momentum and high pseudo-rapidity.

Calculations have been performed at next-to-leading order in the strong coupling constant α_s[8, 9, 13] that include the corrections to the top quark decay as well as preserve spin correlations[14–16]. Figures 2 and 3 show the transverse energy (E_T) and pseudo-rapidity (η *) distributions of the final state jets, for both the s-channel and the t-channel. The events in these histograms have passed selection cuts similar to those used in the experimental analysis below: exactly one lepton with $E_T >$ 15 GeV, missing transverse energy $\not\!\!E_T > 15$ GeV, and at least two jets with $E_T > 15$ GeV. Only events in which a t quark (not $\bar{t}$) is produced are included in the plots, and only the electron decay mode of the W boson.

It can be seen from Fig. 2 that the s-channel final state jets all appear in the central pseudo-rapidity region, and that all, except for the gluon jet, are at high transverse energy. This gluon jet is not present at tree level but only in the $O(\alpha_s)$ correction with real emission. About a third of the events in the s-channel contain such a jet

* Pseudo-rapidity is defined as $\eta = -\ln(\tan\frac{\theta}{2})$, where θ is the polar angle with origin at the primary vertex.

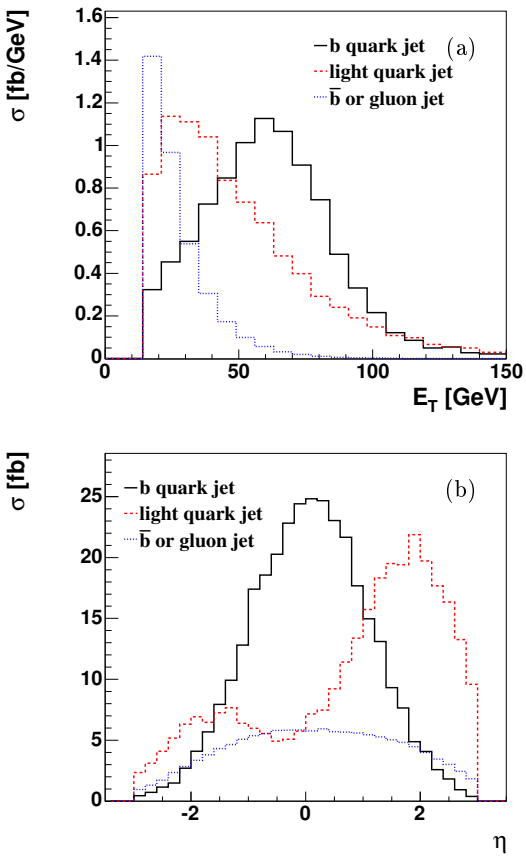

Figure 3: Transverse energy (a) and pseudo-rapidity (b) distribution of final state jets at NLO for the t-channel, after selection cuts.

for the given set of cuts.

Figure 3 shows the same kinematic distributions for the t-channel process. Again, the b quark jet from the top quark decay appears at central rapidities and high E_T. The light quark jet, produced with the top quark, is also at high E_T, but it appears at more forward pseudo-rapidities, roughly following the initial state light quark. The additional radiation in the t-channel consists either of a gluon jet radiated off the b or light quark, or of a $\bar{b}$ quark jet from initial state gluon splitting into a $b\bar{b}$ quark pair, as shown in Fig. 1 (b). This additional radiation is at low E_T and spreads out to higher pseudo-rapidities than the top quark decay products. About 40% of the t-channel events contain such an additional jet for the given set of cuts.

Figures 2 and 3 show that in order to maximize the acceptance for single top quark events, the E_T and η cuts on the jets have to be kept as loose as possible. They also show, however, that at these low E_T thresholds, the $O(\alpha_s)$ correction have a large impact on single top quark events and in particular, not only 2-jet events, but also 3-jet events should be included in the analysis.

DØ DETECTOR

The DØ detector has a central-tracking system, consisting of a silicon microstrip tracker (SMT) and a central fiber tracker (CFT), both located within a 2 T superconducting solenoidal magnet [17], with designs optimized for tracking and vertexing at pseudo-rapidities $|\eta| < 3$ and $|\eta| < 2.5$, respectively. A liquid-argon/uranium calorimeter has a central section (CC) covering pseudo-rapidities $|\eta|$ up to ≈ 1.1, and two end calorimeters (EC) that extend coverage to $|\eta| \approx 4.2$, with all three housed in separate cryostats [18]. An outer muon system, at $|\eta| < 2$, consists of a layer of tracking detectors and scintillation trigger counters in front of 1.8 T toroids, followed by two similar layers after the toroids. Luminosity is measured using plastic scintillator arrays placed in front of the EC cryostats. Trigger and data acquisition systems are designed to accommodate the high luminosities of Run II. Based on preliminary information from tracking, calorimetry, and muon systems, the output of the first level of the trigger is used to limit the rate for accepted events to ≈ 2 kHz. At the next trigger stage, with more refined information, the rate is reduced further to ≈ 1 kHz. These first two levels of triggering rely mainly on hardware and firmware, with the second level also employing software algorithms for event reconstruction and trigger decisions. The third and final level of the trigger, with access to all the event information, uses software algorithms and a computing farm, and reduces the output rate to ≈ 50 Hz, which is written to tape.

SINGLE TOP QUARK EVENT SELECTION

The search for single top quark production is performed using a dataset of 230pb^{-1} collected with the DØ detector. Signal-like events are selected containing a high-E_T lepton, $\not\!\!E_T$, and at least two jets. The analysis is separated by W boson decay mode into the electron channel and the muon channel, and by b-quark tag multiplicity into single-tagged and double-tagged events, resulting in four independent analysis datasets each for the s-channel and t-channel searches.

Event Selection at the Trigger Level

At the trigger level, electron channel events are selected by requiring at least one electromagnetic (EM) object and at least one jet object at each trigger level. Muon channel events are selected by requiring at least one muon object and at least one jet at each trigger level. Details about the trigger conditions at each trigger level are shown in Table I.

The efficiency for single top quark events to pass these trigger conditions is identical for the s-channel and the t-

Table I: Trigger selection for the first part of the data taking period. No E_T cut is applied on the muon, but the muon trigger has an implicit reconstruction threshold of $E_T > 3$GeV because muons have to traverse the muon detector in order to fire the trigger. The trigger conditions and thresholds were adjusted slightly for the second part of the data taking period.

	Electron channel	Muon channel
L1 EM/Muon	$\geq$ 1 EM objects, $E_T > 10$GeV	≥ 1 muon object
Jet	$\geq$ 1 jet objects, $E_T > 10$GeV	$\geq$ 1 jet objects, $E_T > 5$GeV
L2 EM/Muon	$\geq$ 1 EM objects, $E_T > 10$GeV	≥ 1 muon object
Jet	$\geq$ 1 jet objects, $E_T > 10$GeV	-
L3 EM/Muon	$\geq$ 1 EM objects, $E_T > 15$GeV	-
Jet	$\geq$ 1 jet objects, $E_T > 15$GeV	$\geq$ 1 jet objects, $E_T > 20$GeV

channel, about 85% for electron events and 89% for muon events.

Event Selection

In order to maximize the acceptance for single top quark events, the following cuts are made to select events containing a W boson and jets. In the electron channel, exactly one isolated electron is required with $E_T >$ 15 GeV and $|\eta| < 1.1$. In the muon channel, events are selected by requiring exactly one isolated muon with $p_T > 15$ GeV and $|\eta| < 2.0$. Leptons are required to be isolated from jets by a distance of $R > 0.5$, where $R = \sqrt{(\Delta\eta)^2 + (\Delta\phi)^2}$, $\Delta\eta$ is the pseudo-rapidity difference and $\Delta\phi$ the azimuthal angle difference between the two objects . For both channels, events are also required to have $\not\!\!E_T > 15$ GeV. Following the parton-level analysis presented above, events must have from two to four jets with the leading jet $E_T > 25$ GeV and $|\eta| < 2.5$, and all other jets having $E_T > 15$ GeV and $|\eta| < 3.4$. Jets are defined using a cone algorithm with radius $R = 0.5$. Mis-reconstructed events are rejected if they have low $\not\!\!E_T$ and the $\not\!\!E_T$ vector is aligned or anti-aligned in azimuth with the lepton or the jets.

The fraction of signal-like events is further enhanced through the selection of b-quark jets that are identified by reconstructing displaced vertices of long-lived particles inside the jet [19]. At least one jet is required to be b-tagged in this fashion in each event In addition, at least one non-b-tagged jet is required in each event for the t-channel search.

These requirements (excluding b-tagging) select about 23% of the s-channel events and about 22% of the t-channel events (averaged over electrons and muons). The probability to find at least one b-tagged jet is 54% for the s-channel and 38% for the t-channel. The efficiency in the s-channel is higher than in the t-channel because of the presence of two high-E_T b-quark jets in the former. These acceptances are estimates from Monte Carlo simulated events based on the CompHEP generator [20].

Table II: Estimates for signal and background yields and the number of observed events in data passing the selection cuts for the electron and muon channels combined, requiring at least one b-tagged jet. The W+jets row also includes di-boson events. The total background for the s-channel (t-channel) search includes the background from t-channel (s-channel) production.

	s-channel search	t-channel search
s-channel	5.5	
t-channel		8.5
W+jets	169	164
$t\bar{t}$	78	76
multijet	31	31
Total background	287 ± 44	276 ± 41
Observed events	283	271

Event Yields

There are several background processes that mimic the single top quark event signature. The dominant background that is hardest to beat down is from W boson production in association with jets. The second largest background contribution comes from $t\bar{t}$ production, both in the lepton+jets and di-lepton decay modes. Smaller backgrounds are from QCD multijet production where one of the jets is mis-identified as an isolated lepton, and from di-boson events (WW and WZ). The shapes of the W+jets, $t\bar{t}$, and di-boson backgrounds are estimated from Monte Carlo simulation, while the shape of the multijet background is estimated from a data sample enriched in multijet events. The numbers of expected W+jets and multijet events are normalized to the data sample before requiring a b-tag, and the $t\bar{t}$ and di-boson samples are normalized to theoretically predicted yield. The fraction of W+jets events containing heavy flavor jets (Wbb/Wjj) is normalized to the NLO value, calculated with the MCFM program [21].

The event yields in each search after the selection cuts for the signals and the various backgrounds are listed in Table II. Though we expect there to be some single top events left after selection cuts, they are buried by the huge backgrounds. The signal:background ratio is 1:52 in the s-channel search and 1:32 in the t-channel search, making an extraction of the signal out of the large backgrounds a daunting task.

Table III: Dominant contributions to the systematic uncertainty on the acceptance and normalization of the signal and background samples for each b-tag multiplicity.

Source	single-tagged	double-tagged
Acceptance		
b-tag modeling	10%	20%
jet energy scale	8%	15%
jet identification	5%	10%
trigger modeling	6%	6%
jet fragmentation	5%	5%
lepton identification	4%	4%
Normalization		
Theory cross sections	18%	18%
W+jets flavor composition	5%	15%
luminosity	6.5%	6.5%

The most important sources of systematic uncertainty on the signal acceptance and background normalization are listed in Table III. The systematic uncertainty on the shapes of the distributions is also taken into account. We include contributions from b-tag modeling, jet energy scale, jet identification, and trigger modeling. Systematic uncertainties are evaluated for the Monte Carlo signal and background samples, separately for the electron and muon channels and for each b-tag multiplicity. The total uncertainty on the signal acceptance for single-tagged events is 13% for the s-channel and 15% for the t-channel, and for double-tagged events it is 24% for the s-channel and 28% for the t-channel. The total uncertainty on the background yield is 10% for the single-tagged samples and 26% for the double-tagged samples.

We can calculate production cross section limits after event selection to get an idea of the sensitivity of the analysis at this stage. Including all systematic uncertainties and their correlations, the corresponding limits on the production cross section at the 95% confidence level (C.L.) are 13.0 pb in the s-channel and 13.6 pb in the t-channel. It is clear that in order to improve on these limits, we will have to go beyond event counting and need to take advantage of kinematic variables to separate the signals from the backgrounds.

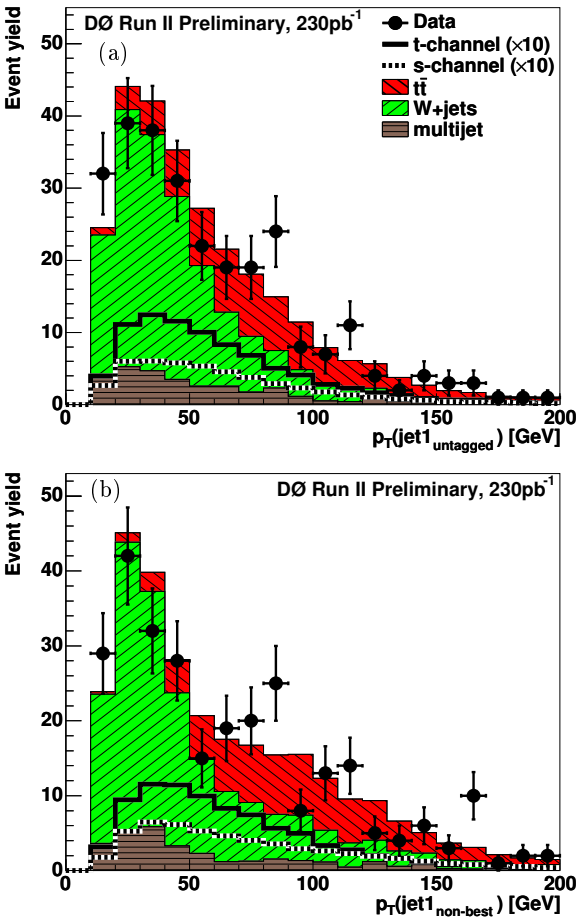

Figure 4: Comparison of signal, background, and data for the electron and muon channels combined, requiring at least one tag, for two important object kinematic variables. Shown are (a) the transverse momentum of the leading untagged jet, and (b) the transverse momentum of the leading non-best jet. Signals are multiplied by ten for readability.

DISCRIMINATING VARIABLES

Further steps beyond event selection are required to extract the single top quark signals from the overwhelming backgrounds. In this section, we present important kinematic variables that allow us to separate the s-channel and t-channel signals from the backgrounds.

The detailed study of single top quark production at NLO [15, 16], together with an analysis of Feynman diagrams of signals and backgrounds [22], forms the basis for the list of discriminating variables used in this analysis. To maximize the signal-background separation, properties of the final state top quark can be exploited, such as the large top quark mass, kinematic distributions of the top quark decay products, or top quark spin correlations. In order to do so, it is important to identify the decay products of the top quark in each event with high efficiency. In this analysis, the W boson is reconstructed from the isolated lepton and the missing transverse energy. The z-component of the neutrino momentum (p_z^ν) is calculated using a W boson mass constraint, choosing the solution with smaller $|p_z^\nu|$ from the two possible solutions. The assignment of final state jets to either the b quark from the top quark decay and the other quark is done differently for the s-channel and t-channel because of the different final state objects. In the s-channel analysis, the final state contains two high-E_T b quarks, and only one of them is typically identified through b-tagging. Thus, b-tagging information is not used in the s-channel to identify the b quark from the top quark decay. The top quark is instead reconstructed from the W boson and the

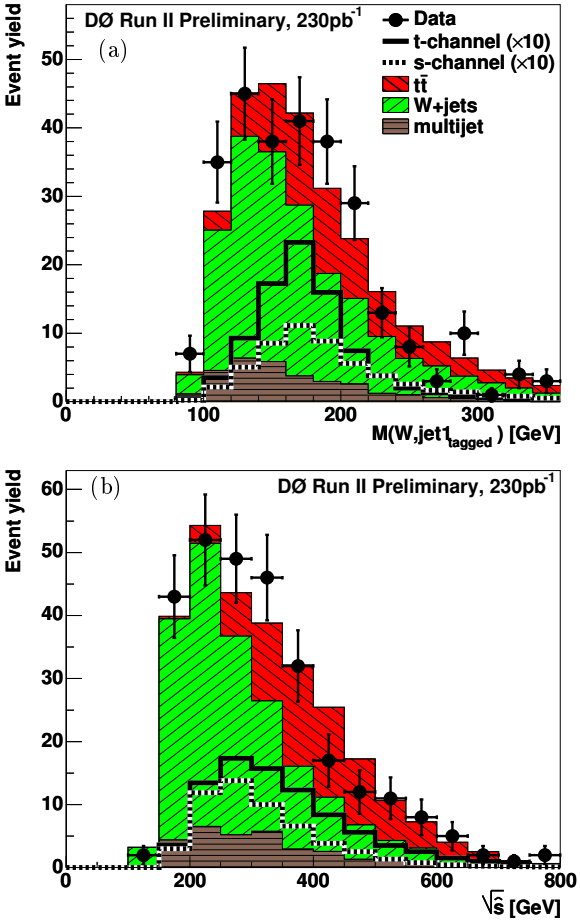

Figure 5: Comparison of signal, background, and data for the electron and muon channels combined, requiring at least one tag, for two important event kinematic variables. Shown are (a) the invariant mass of the top quark reconstructed from the W boson and the leading tagged jet and (b) the invariant mass of all final state objects. Signals are multiplied by ten for readability.

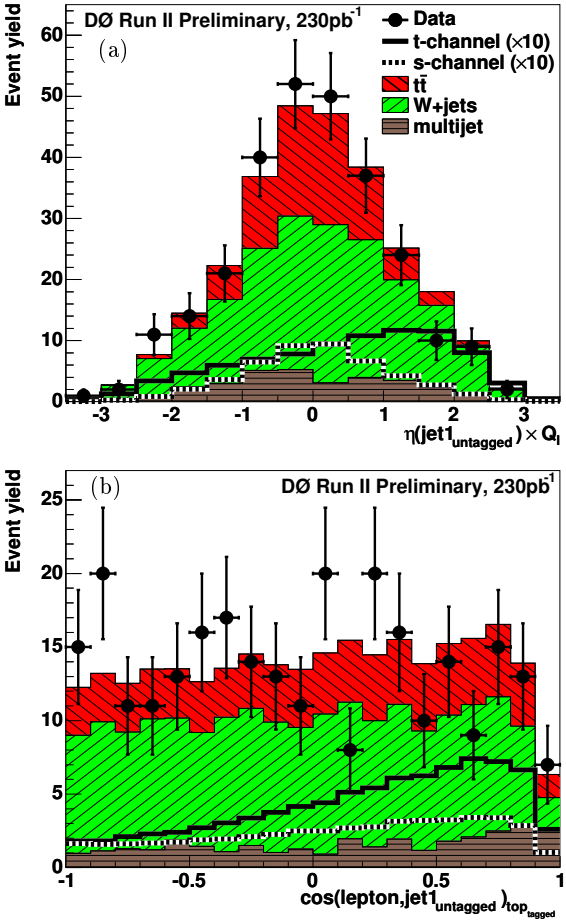

Figure 6: Comparison of signal, background, and data for the electron and muon channels combined, requiring at least one tag, for two important angular variables. Shown are (a) the pseudo-rapidity of the leading untagged jet, corrected for the lepton charge, and (b) the angular correlation between the lepton and the leading untagged jet in the top quark rest frame. Signals are multiplied by ten for readability.

"best" jet [11]. The best jet is defined as the jet in each event for which the invariant mass of the reconstructed W boson and jet is closest to $m_t = 175$GeV. The $\bar{b}$ quark produced together with the top quark is identified as the leading "non-best" jet.

In contrast to the s-channel, there is typically only one high-E_T b quark in the t-channel final state, which is easily identified as the b-tagged jet. Thus, the top quark is reconstructed from the W boson and the leading b-tagged jet in the t-channel. The light quark is identified as the leading non-b-tagged (or untagged) jet. Using these two methods we are able to identify the b-quark jet originating from the top quark decay correctly in about 90% of the single top quark signal events.

The list of discriminating variables is based on these reconstructed final state objects. The variables fall into three categories: individual-object kinematics (jet p_T), global-event kinematics (reconstructed masses and sums of jet energies for various jet combinations), and angular correlations (jet angular separation and top quark spin correlations).

Two of the important individual-object kinematic variables are shown in Fig. 4. They exploit the difference in jet E_T between the W+jets background, for which jets are typically at lower E_T, and the single top signals, for which jets are typically at higher E_T, see also Figs. 2 (a) and 3 (a).

These differences in individual jet energies are also reflected in global-event kinematic variables such as the total energy H or the total transverse energy H_T of various combinations of jets. Other global-event kinematic variables take advantage of the presence of a heavy top quark in the final state, such as the invariant mass of the reconstructed top quark. Two of the important global-event kinematic variables are shown in Fig. 5.

Table IV: Input variables for the neural network analysis. The check marks indicate for which signal-background pair each variable shows discrimination, i.e. in which neural network each variable is used.

Variable	Description	Signal-Background Pairs: s-channel $Wb\bar{b}$	s-channel $t\bar{t}$	t-channel $Wb\bar{b}$	t-channel $t\bar{t}$
	Object kinematics				
$E_T(\text{jet1}_{\text{tagged}})$	Transverse energy of the leading tagged jet	√	√	√	—
$E_T(\text{jet1}_{\text{untagged}})$	Transverse energy of the leading untagged jet	—	—	√	√
$E_T(\text{jet2}_{\text{untagged}})$	Transverse energy of the second untagged jet	—	—	—	√
$E_T(\text{jet1}_{\text{nonbest}})$	Transverse energy of the leading non-best jet	√	√	—	—
$E_T(\text{jet2}_{\text{nonbest}})$	Transverse energy of the second non-best jet	√	√	—	—
	Event kinematics				
$M_T(\text{jet1}, \text{jet2})$	Transverse mass of the two leading jets	√	—	—	—
$p_T(\text{jet1}, \text{jet2})$	Transverse momentum of the two leading jets	√	—	√	—
$M(\text{alljets})$	Invariant mass of all jets	√	√	√	√
$H_T(\text{alljets})$	Sum of the transverse energies of all jets	—	—	√	—
$M(\text{alljets} - \text{jet1}_{\text{tagged}})$	Invariant mass of all jets excluding the leading tagged jet	—	—	—	√
$H(\text{alljets} - \text{jet1}_{\text{tagged}})$	Sum of the energies of all jets excluding the leading tagged jet	—	√	—	√
$H_T(\text{alljets} - \text{jet1}_{\text{tagged}})$	Sum of the transverse energies of all jets excluding the leading tagged jet	—	—	—	√
$p_T(\text{alljets} - \text{jet1}_{\text{tagged}})$	Transverse momentum of all jets excluding the leading tagged jet	—	√	—	√
$M(\text{alljets} - \text{jet}_{\text{best}})$	Invariant mass of all jets excluding the best jet	—	√	—	—
$H(\text{alljets} - \text{jet}_{\text{best}})$	Sum of the energies of all jets excluding the best jet	—	√	—	—
$H_T(\text{alljets} - \text{jet}_{\text{best}})$	Sum of the transverse energies of all jets excluding the best jet	—	√	—	—
$M(W, \text{jet1}_{\text{tagged}})$	Invariant mass of the reconstructed top quark using the leading tagged jet	√	√	√	√
$M(W, \text{jet}_{\text{best}})$	Invariant mass of the reconstructed top quark using the best jet	√	—	—	—
$\sqrt{\hat{s}}$	Invariant mass of all final state objects	√	—	√	√
	Angular variables				
$\Delta R(\text{jet1}, \text{jet2})$	Angular separation between the leading two jets	√	—	√	—
$\eta(\text{jet1}_{\text{untagged}}) \times Q_\ell$	Pseudo-rapidity of the leading untagged jet × lepton charge	—	—	√	√
$\cos(\ell, Q_\ell \times z)_{\text{top}_{\text{best}}}$	Top quark spin correlation in the optimal basis in the s-channel [23], reconstructing the top quark with the best jet	√	—	—	—
$\cos(\ell, \text{jet1}_{\text{untagged}})_{\text{top}_{\text{tagged}}}$	Top quark spin correlation in the optimal basis in the t-channel [23], reconstructing the top quark with the leading tagged jet	—	—	√	—
$\cos(\text{alljets}, \text{jet1}_{\text{tagged}})_{\text{alljets}}$	Cosine of the angle between the leading tagged jet and the alljets system in the alljets rest frame	—	—	√	√
$\cos(\text{alljets}, \text{jet1}_{\text{nonbest}})_{\text{alljets}}$	Cosine of the angle between the leading non-best jet and the alljets system in the alljets rest frame	—	√	—	—

The top quark spin angular correlation variables rely in particular on the accurate reconstruction of the final state top quark, for example the top quark spin correlation in the optimal basis in the t-channel, shown in Fig. 6 (a). Another important angular variable is the asymmetric pseudo-rapidity of the light quark in the t-channel, shown in Fig. 6 (b) (see also Fig. 3 (b)). Other angular variables exploit the difference in jet angles between the W+jets background where jets from gluon splitting tend to be close together and the single top quark signal, where jets tend to be well separated.

OPTIMIZED EVENT ANALYSIS

Each of the variables we have studied provides some discrimination between signal and background, however, because none is sufficiently powerful on its own, it is necessary to combine them in an optimal way. When combining several discriminating variables in neural networks, the signal-background separation improves dramatically. We have chosen to optimize networks separately for the s-channel and the t-channel and to focus on separating the single top signals from the two largest backgrounds: W+jets (using a $Wb\bar{b}$ MC sample for training) and $t\bar{t}$ (using a $t\bar{t} \to \ell$+jets MC sample for training). The neural networks used in this analysis are composed of three layers of nodes: an input layer, a hidden layer, and an output layer. The MLPFIT package is used for training and testing [24], using event sets created from the signal and background simulated samples. The number of hidden nodes and the input variables to each network are chosen in an optimization procedure based on maximizing signal-background separation in an independent test sample.

Table IV lists the variables used in each of the resulting four neural networks.

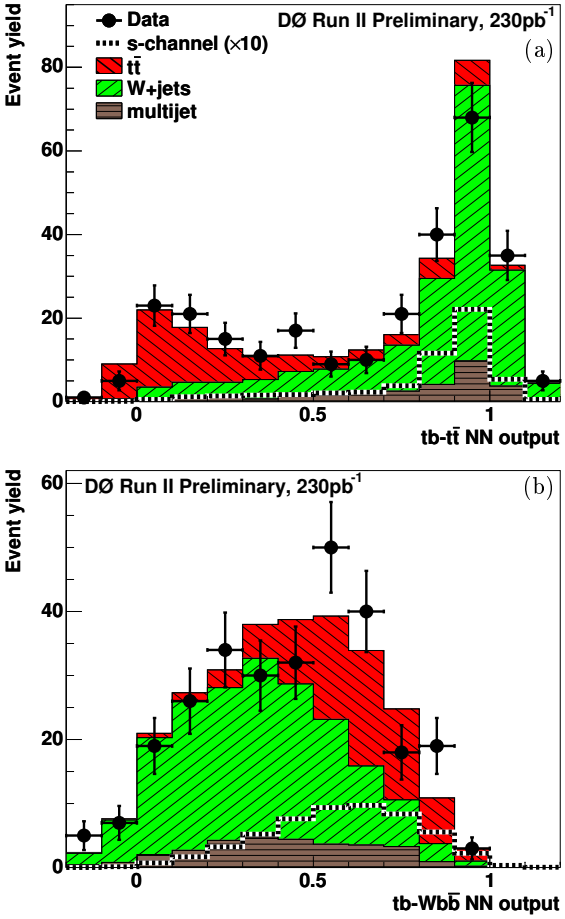

Figure 7: Comparison of signal, background, and data for the electron and muon channels combined, requiring at least one tag, for the neural network outputs for the s-channel (tb) search. Shown are the outputs for (a) $tb - t\bar{t}$, (b) $tb - Wb\bar{b}$. Signals are multiplied by ten for readability.

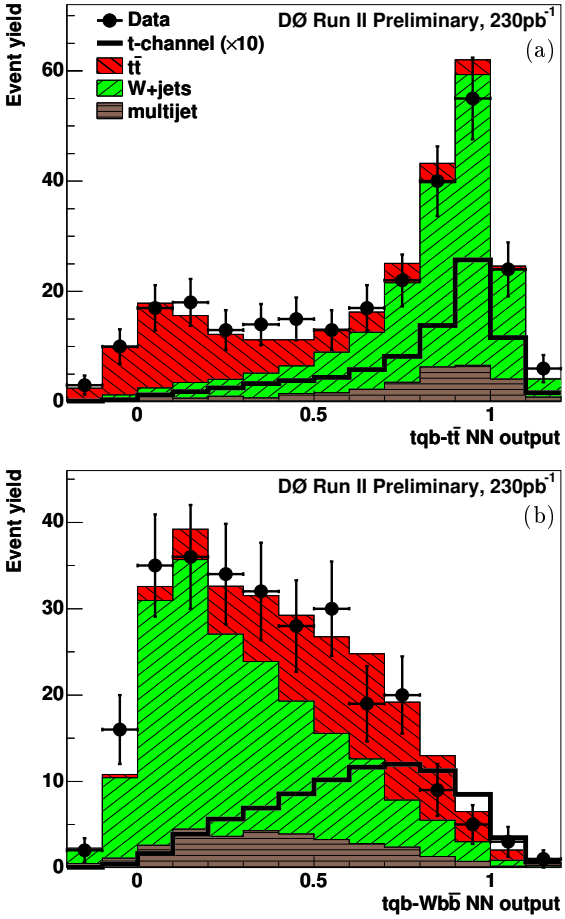

Figure 8: Comparison of signal, background, and data for the electron and muon channels combined, requiring at least one tag, for the neural network outputs for the t-channel (tqb) search. Shown are the outputs for (a) $tqb - t\bar{t}$, (b) $tqb - Wb\bar{b}$. Signals are multiplied by ten for readability.

Neural Network Result

The output of the neural networks for the combined sample of electron and muon, single tagged and double tagged events, is shown in Fig. 7 for the s-channel, and in Fig. 8 for the t-channel. The neural network outputs are around one for signal and around zero for background, but they are not constrained to the interval $[0, 1]$ in MLPFIT. As expected, the neural networks are able to separate the single top quark signals more effectively than any of the individual kinematic variables. The networks separate signal and $t\bar{t}$ backgrounds efficiently, but give less separation for W+jets, where the event kinematics are similar between signal and background.

Figures 7 and 8 show that the background model reproduces the data very well in the background-dominated region around neural network output values close to zero. They also show that there is no excess of events in the region close to one, indicating that there is no evidence for a single top quark signal.

STATISTICAL ANALYSIS

The observed data are consistent with the background predictions for all analysis channels. We therefore set upper limits on the single top quark production cross section. We do this separately in the s-channel and t-channel searches using a Bayesian approach. In each search, two-dimensional histograms are constructed from the $Wb\bar{b}$ vs. $t\bar{t}$ neural network outputs. A likelihood is built from these histograms for signal, background, and data, as a product over all channels (electron and muon, single and double tags) and all bins. A Poisson distribution is assumed for the observed number of events in each bin and a flat prior probability for the signal cross section. The prior for the combined signal acceptance and background yields is a multivariate Gaussian with uncertainties and correlations described by a covariance

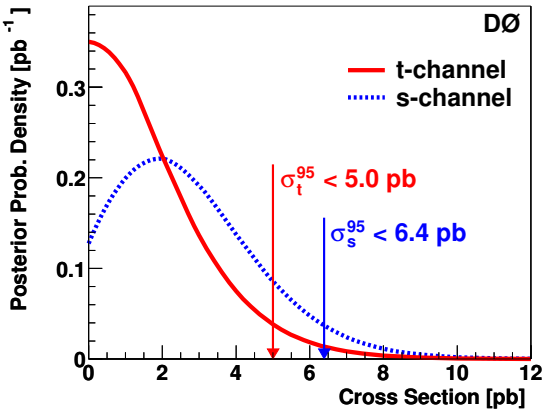

Figure 9: The Bayesian posterior probability density as a function of the single top quark cross section for the s-channel and t-channel searches.

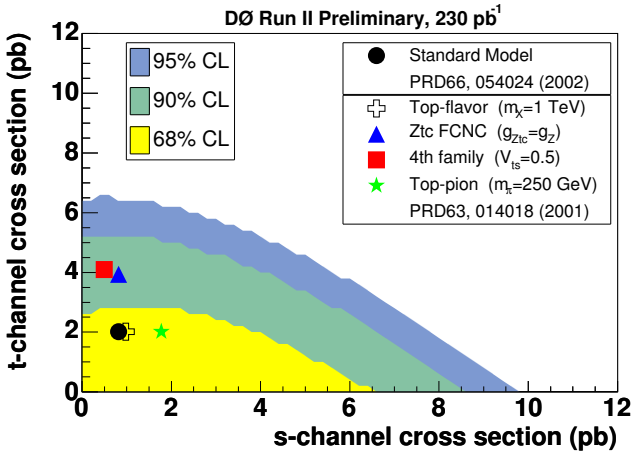

Figure 10: Exclusion contours at 68%, 90%, and 95% confidence level on the posterior density distribution as a function of both the s-channel and t-channel cross sections. The s-channel likelihood is obtained from s-channel muon data only and the t-channel likelihood from t-channel electron channel data only, such that the two likelihoods are independent. Also shown are the NLO prediction from Ref. [8] as well as several representative new physics contributions from Ref. [3].

matrix.

The Bayesian posterior probability densities are shown in Fig. 9 for both the s-channel and t-channel searches. The posterior density peaks at zero for the t-channel, indicating that there is no excess of data events over the background sum. For the s-channel, the posterior density peaks at a value of around 2 pb, indicating that there is a small excess of data events over the background sum. However, the peak is very broad and less than one standard deviation away from zero. This implies that the data are also consistent with the background sum in the s-channel search. The corresponding upper limits on the production cross sections at the 95% confidence level (C.L.) are 6.4 pb in the s-channel and 5.0 pb in the t-channel.

The sensitivity of these measurements is given by the expected upper limits, which are obtained by setting the observed number of events to the background prediction. The expected upper limits are 4.5 pb in the s-channel search and 5.8 pb in the t-channel search. The improvement in sensitivity compared to the limits after event selection is due to the use of a multivariate approach and shape information.

SUMMARY

No evidence is found for electroweak production of single top quarks in 230 pb^{-1} of data collected with the DØ detector at $\sqrt{s}$ = 1.96TeV. A secondary-vertex reconstruction algorithm has been employed to select events with exactly one, or more than one, b jet in electron+jets and muon+jets final states. Upper limits at the 95% confidence level on the cross section for the s-channel and t-channel processes have been set using a binned likelihood built from the output variables of two neural networks. The s-channel limit of 6.4 pb and the t-channel limit of 5.0 pb improve upon previously published limits by a factor of two. They are also close to the region of sensitivity to models of new physics, such as the presence of an extra heavy boson or a flavor-changing neutral-current vertex [3], as shown in Fig. 10. In particular the t-channel limit is only a factor 2.5 above the cross section value expected from the standard model.

The analysis presented here will be sensitive to standard model single top quark production at integrated luminosities of around 3 fb^{-1}, proving that a discovery of single top quark production in Run II at the Tevatron is well within reach. This is the first time than an experimental analysis has reached the sensitivity required to be able to observe single top quark production in Run II. Larger datasets than the 230 pb^{-1} presented here are currently being analyzed, and we are continually making improvements to all aspects of the analysis. As a result, we are reaching the threshold of discoveries at the Tevatron and the next two years promise to be exciting times for top quark electroweak physics.

I thank the DØ single top working group and top physics groups and everyone else who contributed to this result and provided their help for this writeup.

* Electronic address: schwier@fnal.gov

[1] F. Abe et al. (CDF collaboration), Phys. Rev. Lett. **74**, 2626 (1995), hep-ex/9503002.

[2] S. Abachi et al. (D0 collaboration), Phys. Rev. Lett. **74**, 2632 (1995), hep-ex/9503003.

[3] T. Tait and C.-P. Yuan, Phys. Rev. **D63**, 014018 (2001), hep-ph/0007298.

[4] A. Stange, W. J. Marciano, and S. Willenbrock, Phys. Rev. **D49**, 1354 (1994), hep-ph/9309294.

[5] A. Stange, W. J. Marciano, and S. Willenbrock, Phys. Rev. **D50**, 4491 (1994), hep-ph/9404247.

[6] A. Belyaev, E. Boos, and L. Dudko, Mod. Phys. Lett. **A10**, 25 (1995), hep-ph/9510399.

[7] Q.-H. Cao, S. Kanemura, and C.-P. Yuan, Phys. Rev. **D69**, 075008 (2004), hep-ph/0311083.

[8] B. W. Harris, E. Laenen, L. Phaf, Z. Sullivan, and S. Weinzierl, Phys. Rev. **D66**, 054024 (2002), hep-ph/0207055.

[9] Z. Sullivan, Phys. Rev. **D70**, 114012 (2004), hep-ph/0408049.

[10] D. Acosta et al. (CDF), Phys. Rev. **D69**, 052003 (2004).

[11] B. Abbott et al. (DØ), Phys. Rev. **D63**, 031101 (2001), hep-ex/0008024.

[12] D. Acosta et al. (CDF), Phys. Rev. **D71**, 012005 (2005).

[13] J. Campbell, R. K. Ellis, and F. Tramontano, Phys. Rev. **D70**, 094012 (2004), hep-ph/0408158.

[14] Q.-H. Cao and C. P. Yuan, Phys. Rev. **D71**, 054022 (2005), hep-ph/0408180.

[15] Q.-H. Cao, R. Schwienhorst, and C. P. Yuan, Phys. Rev. **D71**, 054023 (2005), hep-ph/0409040.

[16] Q.-H. Cao, R. Schwienhorst, J. Benitez, R. Brock, and C.-P. Yuan, submitted to Phys. Rev. **D** (2005), hep-ph/0504230.

[17] V. Abazov et al. (D0 collaboration), in preparation for submission to Nucl. Instrum. Methods Phys. Res. **A** (2005).

[18] S. Abachi et al. (D0), Nucl. Instrum. Meth. **A338**, 185 (1994).

[19] V. Abazov et al. (D0 collaboration), in preparation for submission to Phys. Rev. Lett. (2005).

[20] E. Boos et al. (CompHEP), Nucl. Instrum. Meth. **A534**, 250 (2004), hep-ph/0403113.

[21] J. Campbell and R. K. Ellis, Phys. Rev. **D65**, 113007 (2002), hep-ph/0202176.

[22] E. Boos and L. Dudko, Nucl. Instrum. Meth. **A502**, 486 (2003), hep-ph/0302088.

[23] G. Mahlon and S. J. Parke, Phys. Rev. **D53**, 4886 (1996), hep-ph/9512264.

[24] J. Schwindling, http://schwind.home.cern.ch/schwind/MLPfit.ht (2000).